Measurement of the 183 keV resonance in $^{17}O(p,\alpha)^{14}N$ using a novel technique

B. H. Moazen,[1,2] D. W. Bardayan,[1] J. C. Blackmon,[1] K. Y. Chae,[1,2] K. Chipps,[3] C. P. Domizioli,[4] R. Fitzgerald,[5] U. Greife,[3] W. R. Hix,[1,2] K. L. Jones,[2,6] R. L. Kozub,[4] E. J. Lingerfelt,[1,2] R. J. Livesay,[3] C. D. Nesaraja,[1,2] S. D. Pain,[6] L. F. Roberts,[1] J. F. Shriner Jr.,[4] M. S. Smith,[1] and J. S. Thomas[6]

[1]*Physics Division, Oak Ridge National Laboratory, Oak Ridge, Tennessee 37831, USA*
[2]*Department of Physics and Astronomy, University of Tennessee, Knoxville, Tennessee 37996, USA*
[3]*Department of Physics, Colorado School of Mines, Golden, Colorado 80401, USA*
[4]*Department of Physics, Tennessee Technological University, Cookeville, Tennessee 38505, USA*
[5]*Department of Physics and Astronomy, University of North Carolina, Chapel Hill, North Carolina 27599, USA*
[6]*Department of Physics and Astronomy, Rutgers University, Piscataway, New Jersey 08854, USA*

(Received 14 March 2007; published 4 June 2007)

We have developed a novel technique for measurements of low-energy (p,α) reactions using heavy-ion beams and a differentially pumped windowless gas target. We applied this new approach to study the 183 keV resonance in the $^{17}O(p,\alpha)^{14}N$ reaction. We report a (center-of-mass) resonance energy of $E_r = 183.5^{+0.1}_{-0.4}$ keV and a resonance strength of $\omega\gamma_{p\alpha} = (1.70 \pm 0.15)$ meV, and we set an upper limit (95% confidence) on the total width of the state of $\Gamma < 0.1$ keV. This resonance is important for the $^{17}O(p,\alpha)^{14}N$ reaction rate, and we find that ^{18}F production is significantly decreased in low-mass ONeMg novae but less affected in more energetic novae. We also report the first determination of the stopping power for oxygen ions in hydrogen gas near the peak of the Bragg curve ($E = 193$ keV/u) to be $(63 \pm 1) \times 10^{-15}$ eV cm^2.

DOI: 10.1103/PhysRevC.75.065801 PACS number(s): 26.30.+k, 34.50.Bw, 25.70.Ef, 26.20.+f

I. INTRODUCTION

The rates of the $^{17}O(p,\alpha)^{14}N$ and $^{17}O(p,\gamma)^{18}F$ reactions are important for understanding giant stars and novae. Measurements of the ratios of abundances of the oxygen isotopes in the atmospheres of giant stars [1] and in presolar grains [2] provide interesting constraints on mixing in stars approaching the giant branch [3,4]. These abundances have even been used to constrain the age of the Galaxy [5]. The fragile ^{17}O isotope is also abundantly produced in novae, which may be the dominant contributors to ^{17}O production in the Galaxy [6]. The $^{17}O(p,\gamma)^{18}F$ reaction leads to production of ^{18}F, a dominant source of potentially observable γ rays in novae, whereas the $^{17}O(p,\alpha)^{14}N$ reaction bypasses ^{18}F production [7]. The interpretation of measured oxygen isotopic abundance ratios, our understanding of the Galactic origins of ^{17}O, as well as the analysis of γ-ray observations of novae all require an accurate understanding of the $^{17}O(p,\alpha)^{14}N$ and $^{17}O(p,\gamma)^{18}F$ reaction rates.

The properties of a resonance at $E_{\text{c.m.}} = 183$ keV are important for understanding the $^{17}O(p,\alpha)^{14}N$ and $^{17}O(p,\gamma)^{18}F$ reaction rates at temperatures $T \approx (1\text{–}4) \times 10^8$ K relevant for novae and asymptotic giant branch (AGB) stars. The strength of the 183 keV resonance in the $^{17}O(p,\alpha)^{14}N$ reaction was recently directly measured by using a low-energy proton beam at Orsay, and a resonance strength was reported ($\omega\gamma_{p\alpha} = 1.6 \pm 0.2$ meV) [8,9] that was over 50 times greater than that inferred ($\omega\gamma_{p\alpha} < 0.03$ meV) from a measurement of the $^{17}O(p,\gamma)^{18}F$ reaction at Triangle Universities Nuclear Laboratory (TUNL) [10]. A recent measurement of the $^{14}N(\alpha,\gamma)^{18}F$ reaction set a short limit ($\tau < 2.6$ fs) on the lifetime of the corresponding state ($E_x = 5790$ keV in ^{18}F) [9] in contrast to an earlier measurement [11]. Use of the inaccurate lifetime for the 5790 keV state in Ref. [10] likely explains the apparent discrepancy in the inferred (p,α) resonance strength with the results of Refs. [8,9]. The resonance energy is in good agreement between Refs. [10,12] and Refs. [8,9], but the strength for the $^{17}O(p,\gamma)^{18}F$ resonance was found to be 80% larger in Refs. [8,9] than in Refs. [10,12]. The substantially larger strength for the $^{17}O(p,\alpha)^{14}N$ reaction has a particularly significant impact on nucleosynthesis. For example, the abundances of ^{17}O and ^{18}F produced in novae were found to be reduced by a factor of as much as 8 in some novae with the larger $^{17}O(p,\alpha)^{14}N$ reaction rate [8].

We have developed a novel experimental technique that is optimized for the measurement of narrow resonances in (p,α) reactions. In this approach, a heavy-ion beam bombards a differentially pumped target of hydrogen gas, and reaction products are efficiently detected in a large annular array of silicon detectors. A significant advantage of this approach is that the pure nature of the target maximizes the yield from narrow resonances. The target stoichiometry is well known and does not degrade or vary with beam conditions, thus mitigating uncertainties that are encountered when studying narrow resonances in targets of complicated composition. The gas pressure can also be adjusted to match the areal target density to the expected resonance width to minimize the nonresonant background. This approach was developed to achieve high sensitivity for measurements with radioactive ion beams. In this paper we report on a demonstration of this new technique applied to the 183 keV resonance in the $^{17}O(p,\alpha)^{14}N$ reaction that is important in novae and AGB stars.

II. EXPERIMENTAL APPROACH

We measured cross sections for the $^1H(^{17}O,\alpha)^{14}N$ reaction at the Holifield Radioactive Ion Beam Facility (HRIBF) at Oak Ridge National Laboratory (ORNL). Low-energy beams

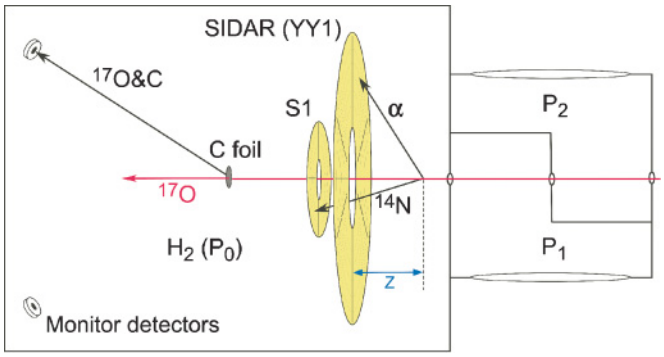

FIG. 1. (Color online) Schematic of the experimental setup. Only two (of four) differential pumping stages are shown.

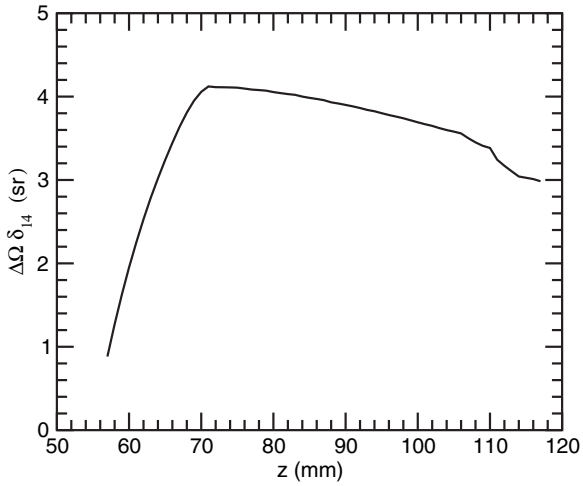

FIG. 2. The total solid angle (center-of-mass frame) for detection of α particles, $\Delta\Omega$, times the efficiency for detection of a coincident ^{14}N recoil, δ_{14}, plotted as a function of z, the distance from the reaction vertex to the plane of the SIDAR array.

of ^{17}O from the HRIBF tandem accelerator with an intensity of about 1 pnA bombarded a large scattering chamber filled with hydrogen gas at a pressure of 4 Torr. The scattering chamber was connected to the accelerator beamline by a series of four differentially pumped chambers separated by 5-mm-diameter apertures. A schematic illustration of the experimental setup is shown in Fig. 1. No windows or foils obstructed the beam or contained the gas, and the hydrogen gas in the scattering chamber served as a spatially extended target for the (p, α) reaction. Ultrahigh purity gas (>99.999% H_2) was used in a single-pass system, with a equivalent gas flow rate of about 70 ml/s (at standard temperature and pressure) to maintain a constant pressure of $P_0 = 4.000$ Torr in the target chamber. The gas pressure in the target chamber was measured by using capacitance diaphragm gauges and regulated to better than $\pm 0.2\%$ throughout the measurements. The pressure in the first differential pumping stage just upstream of the target chamber was reduced to about 5% of the target chamber pressure ($P_1 \approx$ 0.02 Torr) by using roots mechanical pumps. Turbomolecular pumps on the other differential pumping stages reduced the pressure from $P_2 \approx 10^{-4}$ Torr to the beamline pressure of $\approx 10^{-7}$ Torr over a distance of about 30 cm.

The α and ^{14}N reaction products were detected in coincidence by an array of silicon strip detectors operating within the hydrogen gas environment. The annular Silicon Detector Array (SIDAR) [13] was arranged as a single layer of eight type $YY1$ detectors (manufactured by Micron Semiconductor) located at a distance of 115 mm from the entrance to the chamber and normal to the beam axis. The active area of SIDAR has an inner (outer) radius of 50 mm (130 mm), and the array provided a large solid angle for the detection of α particles.

Nitrogen recoils from the ^{1}H(^{17}O,α)^{14}N reaction have laboratory angles $\theta_{\rm lab} < 21^\circ$ and thus pass through the center of SIDAR from any point of origin inside the target chamber. The ^{14}N ions were detected by an annular type $S1$ detector from Micron Semiconductor with an inner (outer) radius of 24 mm (48 mm). The location of the $S1$ detector (13.5 mm downstream of SIDAR) allowed ^{14}N ions to be detected in coincidence with high efficiency. The detector elements were individually calibrated with a ^{244}Cm source at a single location. The total solid angle for detection of α particles from the ^{1}H(^{17}O,α)^{14}N reaction and the efficiency for detecting the corresponding ^{14}N recoil in coincidence were calculated based upon the measured geometry as a function of the position of the vertex of the reaction along the beam axis. In Fig. 2 we plot the integrated solid angle (center-of-mass frame) for detection of the α from the ^{1}H(^{17}O,α)^{14}N reaction, $\Delta\Omega_{\rm c.m.}$, multiplied by the efficiency for detecting the corresponding ^{14}N in coincidence, δ_{14}, as a function of the distance between the reaction vertex and plane of SIDAR, z. The efficiency for detection of ^{14}N ions in coincidence, δ_{14}, is nearly constant at about 96% over most of the range but plummets for positions closer to the $S1$ detector than 70 mm as recoiling ^{14}N ions start to pass through the center of the $S1$ detector.

The kinematics and relative timing of the two detected particles allowed the ^{1}H(^{17}O,α)^{14}N reaction to be cleanly distinguished. The energies of particles detected by the $S1$ detector are plotted against the energy of the coincident particle detected by SIDAR in Fig. 3 for events that are coincident within 0.4 μs. Data taken at bombarding energies of $E(^{17}\text{O}) = 3.29$ MeV (off resonance) and $E(^{17}\text{O}) =$ 3.34 MeV (on resonance) are shown for comparable integrated beam on target. Events from the ^{1}H(^{17}O,α)^{14}N reaction are distinguished as a straight line with a constant sum energy indicative of the reaction Q value and independent of the reaction angle. The two-dimensional gate on the energy-energy plot illustrated in Fig. 3 determined the number of events from the ^{1}H(^{17}O,α)^{14}N reaction, Y.

Each segment of the detector array views reaction products from a wide range of angles depending on the point of origin along the beam axis. However, the reaction angle of each ^{1}H(^{17}O,α)^{14}N event can be determined from the measured α energy, which varies rapidly with angle. In Fig. 4 we plot the reaction yield as a function of the distance from the reaction vertex to the plane of SIDAR, z, that results from the inferred reaction angle and the segmentation of the SIDAR array. All of the ^{1}H(^{17}O,α)^{14}N events originate from a narrow range of positions within the target chamber, indicating that the entire yield is due to a narrow resonance. The incident bombarding energy is plotted in Fig. 5 versus the centroid of the distribution

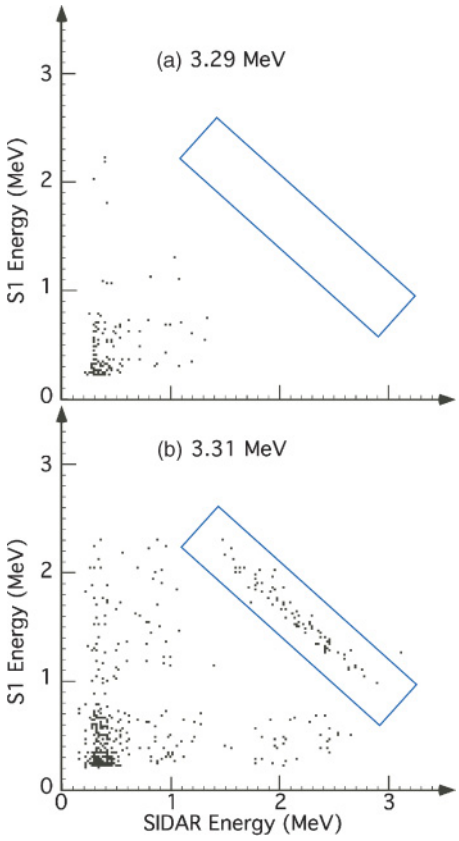

FIG. 3. (Color online) The energy of particles detected in the $S1$ detector plotted versus the energy of coincident particles in SIDAR for (a) $E(^{17}\mathrm{O}) = 3.29$ MeV and (b) $E(^{17}\mathrm{O}) = 3.31$ MeV. Any bins with at least 1 count have a uniform black fill.

of events in z (Fig. 4). The reaction vertex varies linearly with the incident energy, and a least-squares fit to the data determines the stopping power for oxygen ions in hydrogen gas to be $(63 \pm 1) \times 10^{-15}$ eV cm^2 at $E(^{17}\mathrm{O}) = 194$ keV/u. It should be noted that a small energy- and angle-dependent correction was applied to the measured α energy for the estimated energy loss in the 350-nm-thick dead layer on SIDAR and for energy loss in the hydrogen gas (e.g., 6% and 1%, respectively, for a 2 MeV α at $\theta_{\mathrm{lab}} = 45^\circ$) but that energy loss of the incident ^{17}O ($\approx$2% in total) does not significantly contribute since the reaction originates from a well-defined resonance energy.

We also determined the reaction vertex from the coincident ^{14}N recoils in the $S1$ detector using an independent technique. In Fig. 6 we plot the distribution of ^{14}N recoils as a function of the radial strip in the $S1$ detector (y axis) and the detected particle energy (x axis) for $E(^{17}\mathrm{O}) = 3.34$ MeV. A large fraction of the detected ^{14}N recoils are emitted near the maximum laboratory angle of 20.8°. Because of the compression from the center-of-mass to laboratory frame, the angular distribution of the ^{14}N yield provides a good indication of the point of origin of the reaction, whereas the ^{14}N energy is relatively insensitive. We fit the energy-angle distribution of ^{14}N recoils in the $S1$ detector with the calculated distribution by varying only one parameter, the position of the vertex for the $^1\mathrm{H}(^{17}\mathrm{O},\alpha)^{14}\mathrm{N}$ reaction, which was assumed

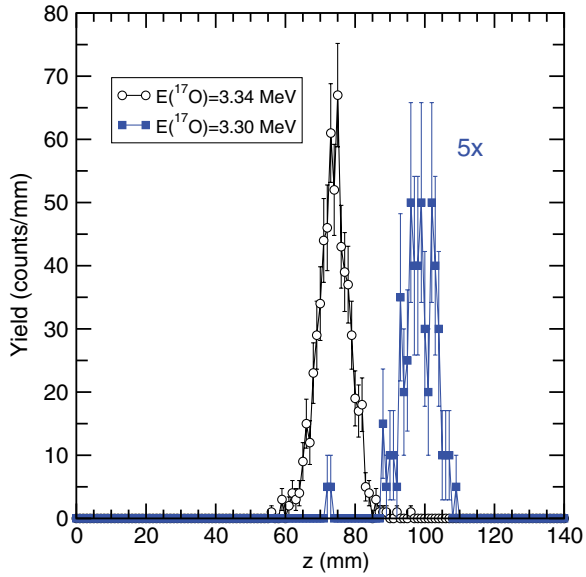

FIG. 4. (Color online) The distribution of $^1\mathrm{H}(^{17}\mathrm{O},\alpha)^{14}\mathrm{N}$ events as a function of the distance from reaction vertex to the plane of SIDAR (z) plotted for incident ^{17}O energies of 3.30 MeV (filled squares) and 3.34 MeV (open circles) at a pressure of 4 Torr. The 3.30 MeV yield has been multiplied by a factor of 5 for comparison.

to be unique for all observed events. The best-fit curve to the data at $E(^{17}\mathrm{O}) = 3.34$ MeV is also shown in Fig. 6. We plot in Fig. 5 the bombarding energy versus the distance from the S1 detector to the reaction vertex determined in this manner. A least-squares fit to the data independently determines the stopping power for oxygen ions in hydrogen gas to be $(64 \pm 3) \times 10^{-15}$ eV cm^2, in good agreement with the value determined from the α particle measurements. We adopt a weighted average from the two techniques and compare our result with two widely used, semi-empirical models [14,15]

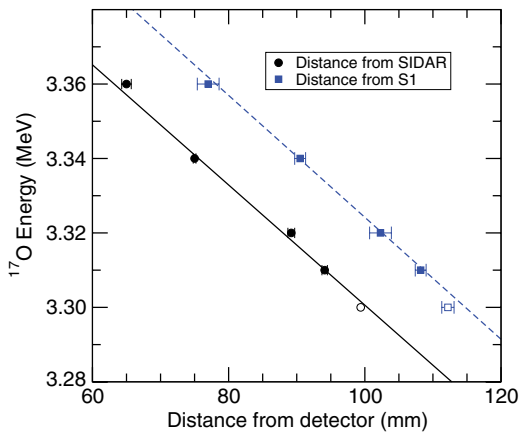

FIG. 5. (Color online) Incident beam energy plotted (circles) versus the distance from the reaction vertex to the plane of the SIDAR, z. The incident beam energy is also plotted (squares) versus the distance from the reaction vertex to the plane of the $S1$ detector as determined by the angular distribution of ^{14}N ions. The lines denote linear fits to the data not including the open data points at the lowest energy that were only partially on resonance.

TABLE I. Results for the stopping power ϵ for oxygen ions in hydrogen gas at 193 keV/u compared to the semi-empirical models SRIM2003 [14] and MSTAR [15].

	ϵ (10^{-15} eV cm^2)
This work	63 ± 1
SRIM2003 [14]	59
MSTAR [15]	53

in Table I. Our stopping power result is interesting in itself since these are the first data for oxygen ions in hydrogen gas at energies near the peak of the Bragg curve.

The integrated beam current at each energy was determined by normalizing to ^{12}C(^{17}O,^{17}O)^{12}C elastic scattering measured simultaneously with the ^{1}H(^{17}O,α)^{14}N reaction by using a carbon foil and two single-collimated silicon surface barrier detectors. The carbon foil was mounted 10 cm downstream of the $S1$ detector inside the hydrogen gas, and the two monitor detectors were mounted about 27 cm from the carbon foil at $\theta_{\rm lab} \approx 33^\circ$ (see Fig. 1). The thickness of the carbon foil was determined to be 32.4 ± 2.0 μg/cm^2 in separate experiments by measuring the energy loss of α particles from a ^{244}Cm source in passing through the foil. The carbon areal target density was deduced by using the stopping power for α particles in carbon from a SRIM fit to experimental data points, $(14.5 \pm 0.8) \times 10^{-15}$ eV cm^2 [14]. Despite the extensive available data, the uncertainty in the α stopping power still dominates the uncertainty in the carbon foil thickness. The solid angles for the collimated monitor detectors (0.417 ± 0.013 and 0.498 ± 0.014 msr) were measured by using a calibrated α source at the position of the carbon foil. A phosphor was mounted on the same target ladder as the carbon foil, and the ^{17}O beam was tuned to this point to achieve reproducible beam conditions at each bombarding energy.

A raw sample spectrum from one of the monitor detectors is shown in Fig. 7. The data from the monitor detectors were prescaled by a factor of 128 to decrease electronics dead time (to less than 5%). Since the elastic scattering used for beam current normalization was subject to the same dead time as

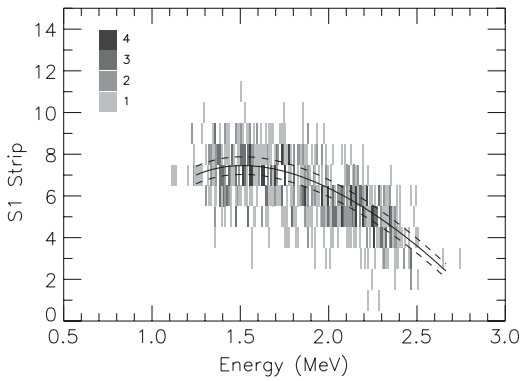

FIG. 6. The distribution of events by ^{14}N angle ($S1$ strip number) and energy (in the $S1$ detector) for events identified as ^{1}H(^{17}O,α)^{14}N for $E(^{17}\text{O}) = 3.34$ MeV. The solid curve shows the best fit to the distribution of ^{14}N recoils varying only the distance to the reaction vertex, z. The dashed curves show the 1σ error band.

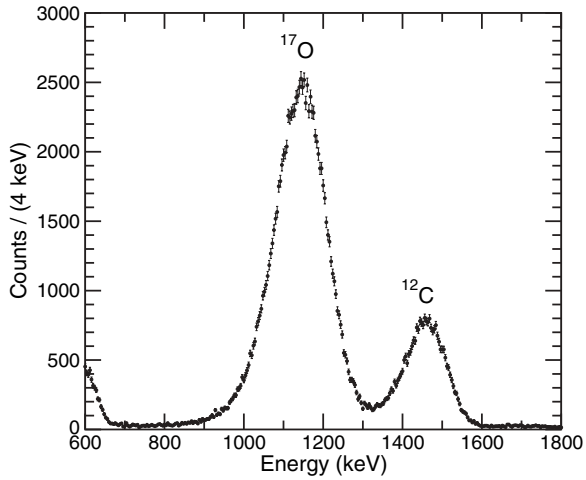

FIG. 7. Raw energy spectrum from one of the monitor detectors. The uncertainties are the statistical uncertainties, $\sqrt{\text{counts}}$.

that for the ^{1}H(^{17}O,α)^{14}N reaction, no correction for dead time was required. The mean scattering angle for each detector was determined from the ratio of ^{17}O and ^{12}C yields and was found to be consistent across all experimental runs to within $\pm 0.5^\circ$. Mean values of 33.0° and 32.4° were adopted for the two detectors, in good agreement with the measured geometry. The number of incident ^{17}O ions was determined from the ^{17}O yield in each monitor detector by using the Rutherford cross section for the ^{12}C(^{17}O,^{17}O)^{12}C reaction at the mean scattering angle determined from the ratio of the ^{12}C and ^{17}O yields. The integrated beam current determined from the two monitor detectors typically differed by between 6% and 8% (and no more than 11%), with one detector indicating a consistently higher beam intensity. We adopt an integrated beam current that is the average of the value from the two detectors and adopt an uncertainty that encompasses values from both monitors.

III. RESULTS

Since the observed yield originates from a narrow resonance, the resonance strength, $\omega\gamma_{p\alpha}$, is well approximated from the thick-target yield on resonance, Y, by

$$\omega\gamma_{p\alpha} = \frac{2}{\lambda^2}\frac{m_p}{m_p + m_{17}} 4\pi\epsilon \left(\frac{Y}{I \int W(\theta_\alpha)\delta_{14}(\theta_\alpha) \sin\theta_\alpha d\theta_\alpha d\phi_\alpha} \right), \quad (1)$$

where λ is the wavelength of the incident ^{17}O ion in the center-of-mass frame at the resonance energy, m_p and m_{17} are the masses of the proton and ^{17}O, respectively, ϵ is the stopping power for ^{17}O ions in hydrogen gas, and I is the total number of incident particles. The integral in the denominator of Eq. (1) is the integral of the solid angle for detection of α particles, $\sin\theta_\alpha d\theta_\alpha d\phi_\alpha$, in the center-of-mass frame, weighted by the angular distribution of α particles, $W(\theta_\alpha)$, and the efficiency for detecting coincident ^{14}N ions, $\delta_{14}(\theta_\alpha)$.

We find the distribution of yield over the center-of-mass angles covered in our measurement ($\theta_{\rm c.m.} = 70^\circ$–$130^\circ$) to be consistent with either an isotropic distribution or with the

distribution

$$W(\theta_\alpha) = 1 + 0.16 P_2(\cos\theta_\alpha)\,, \qquad (2)$$

where $P_2(\cos\theta_\alpha)$ is the second-order Legendre polynomial, as reported by Ref. [8]. Our distribution is slightly better fit by Eq. (2), which varies by less than 10% over the range of angles covered in our measurement. The χ^2 from a fit using the distribution in Eq. (2) is 0.1 lower than that found with an isotropic distribution. Although this is not a statistically significant difference, we adopt Eq. (2) for the angular distribution, which results in a 6% smaller integrated solid angle (and hence a 6% larger resonance strength) than would be obtained by assuming an isotropic distribution.

In Fig. 8, we plot the quantity shown in parentheses in Eq. (1) (the reaction yield, Y, normalized by the incident number of ions, I, and the integrated weighted solid angle) as a function of the incident ^{17}O energy. The uncertainties shown in Fig. 8 include the statistical uncertainty in Y, the uncertainty in the number of incident ions resulting from the two monitor detectors, and the uncertainty in the integrated solid angle that was determined from the width of the distribution of events in distance from SIDAR (Fig. 2). For bombarding energies where insufficient events were observed to determine accurately the reaction vertex (i.e., off resonance), we adopt an upper limit (95% confidence level), shown as triangles in Fig. 8, using the average solid angle for the "on-resonance" data points where a vertex could be accurately determined.

The filled data in Fig. 8 show results of measurements at a pressure of 4 Torr in the target chamber. The beam is expected to experience a small amount of energy loss in the residual hydrogen gas upstream of the entrance aperture to the target chamber. Measurements were also performed with a pressure of 1 Torr in the target chamber to determine the energy loss of the beam before it reaches the sensitive volume and to test the independence of the thick-target reaction yield to gas pressure. Results from measurements at 1 Torr are shown in Fig. 8 as open squares (with the open triangle for an upper limit). Also shown in Fig. 8 are fits to both the 1 Torr and 4 Torr yield curves with varying strength ($\omega\gamma_{p\alpha}$), energy (E_r), and width (Γ) of the resonance. Although the width of the resonance is expected to be quite small, a larger apparent width may result from experimental effects such as the beam energy resolution. However, we find no evidence for a finite width to the resonance and determine an upper limit of $\Gamma < 0.1$ keV (center-of-mass frame) at the 95% confidence level.

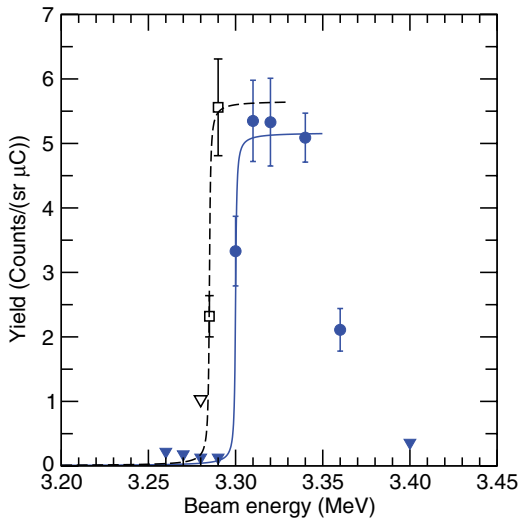

FIG. 8. (Color online) Measured yield curves at 4 Torr (filled circles) and 1 Torr (open squares). Filled (open) triangles denote upper limits at 4 Torr (1 Torr). The solid (dashed) curves are fits to the 4 Torr (1 Torr) data as described in the text.

The resonance strength is mostly independent of the other resonance parameters, and a value of $\omega\gamma_{p\alpha} = (1.70 \pm 0.09)$ meV was obtained from the best fit to the data shown in Fig. 8. The three largest sources of purely systematic uncertainties not included in the data shown in Fig. 8 but that potentially impact the overall normalization of the results are as follows: the thickness of the carbon foil used for beam current normalization (6% arising primarily from the uncertainty in stopping powers for α particles in carbon), the strength of the α source used for efficiency calibrations (3%), and the stopping power for ^{17}O in hydrogen gas (2% as determined in this measurement). Adding each of these uncertainties in quadrature with the result from the fit to the yield curve produces a final result of $\omega\gamma_{p\alpha} = (1.70 \pm 0.15)$ meV.

The best fit to the data at 1 Torr results in a resonance energy that is $\Delta E(^{17}\mathrm{O}) = 15$ keV lower (in the laboratory frame) than the fit at 4 Torr when identical widths are used in both fits. We adopt a value for the resonance energy obtained by a linear extrapolation to zero pressure of the resonance energy obtained from fits to the yield curves with $\Gamma \approx 0$. The result is $\Delta E(^{17}\mathrm{O}) = 20$ keV lower in the laboratory frame ($\Delta E_{\mathrm{c.m.}} = 1.1$ keV lower) than the best-fit value at 4 Torr. The uncertainty in the resonance energy was determined from the extrapolation by including appropriate correlations between the uncertainty in the resonance energy and the uncertainty in the width. Since the observed width may result from experimental effects (e.g., beam energy resolution), and since only upper limits were determined for the off-resonance points and for the width, we find the uncertainty in the resonance energy to be asymmetric, with the final result being $E_r = 183.5^{+0.1}_{-0.4}$ keV.

IV. ASTROPHYSICAL IMPLICATIONS

Our results for the 183 keV resonance in the $^{17}O(p,\alpha)^{14}$N reaction obtained using this new technique ($E_r = 183.5^{+0.1}_{-0.4}$ keV and $\omega\gamma_{p\alpha} = 1.70 \pm 0.15$ meV) are in good agreement with the recent results of Chafa *et al.* ($E_r = 183.2 \pm 0.6$ keV and $\omega\gamma_{p\alpha} = 1.6 \pm 0.2$ meV) [8]. The contribution to the $^{17}\mathrm{O}(p,\alpha)^{14}$N astrophysical reaction rate for this resonance, $N_A\langle\sigma v\rangle_{183\ \mathrm{keV}}$, can be expressed in the narrow, isolated resonance approximation as

$$N_A\langle\sigma v\rangle_{183\ \mathrm{keV}} \approx 276 T_9^{-3/2} \exp(-2.128/T_9)\,, \qquad (3)$$

where T_9 is the temperature in units of 10^9 K, and where we have adopted a weighted average of the current results and those of Ref. [8]. We have calculated the total cross section for the $^{17}\mathrm{O}(p,\alpha)^{14}$N reaction using the R-matrix code SAMMY [16]. Resonance properties were adopted as in Refs. [9] and [17] except for the 183 keV and 530 keV resonances.

TABLE II. The 21 coefficients a_{ij} used to parametrize the $^{17}O(p,\alpha)^{14}N$ rate via a fit of Eq. (4) to the numerically integrated rate. The parametrization is valid over the temperature range 0.01–10 GK and reproduces the rate to within 5% over this range.

$i \backslash j$	1	2	3	4	5	6	7
1	-1.01810×10^{2}	-7.79071×10^{-2}	-1.12473×10^{1}	2.10956×10^{2}	-1.38581×10^{2}	2.32187×10^{1}	-1.34335×10^{1}
2	7.98035×10^{-1}	2.95898×10^{0}	-2.23640×10^{2}	2.40491×10^{2}	-1.04420×10^{1}	4.70954×10^{-1}	-1.36987×10^{2}
3	2.87049×10^{2}	2.70118×10^{-1}	-1.37840×10^{2}	-7.76691×10^{2}	2.22662×10^{3}	-3.08826×10^{3}	-8.66862×10^{1}

For the 183 keV resonance, we adopt a weighted average of the current results with those of Ref. [8]. The contribution of the 530 keV resonance made an insignificant contribution to the total reaction rate recommended in Refs. [9,17]. Since the $E_x = 5.605$ MeV state in ^{18}F (corresponding to an $E_{c.m.} =$ 530 keV resonance in $^{17}O + p$) is identified to have $J^{\pi} = 0^{+}$ [18] and is forbidden by energy and angular momentum selection from undergoing α decay to states in ^{14}N, we adopt $\omega\gamma_{p\alpha} = 0$ for the 530 keV resonance. For other states where the resonance parameters used in Refs. [9] and [17] differ, we adopt the more recent parameters of Ref. [9].

The reaction rate was calculated by numerically integrating the calculated cross section using SAMMY. At high temperatures we match to statistical model calculations following the procedure of Ref. [17]. We find a total reaction rate that is in good agreement with the recommended rate of Ref. [9] for $3 \times 10^{7} < T < 1.5 \times 10^{9}$ K, differing by at most 4% near 2×10^{8} K owing to the slightly higher strength we adopt for the 183 keV resonance. Our rate is also in good agreement with Ref. [17] for $T > 5 \times 10^{8}$ K, differing by less than 4%.

We have parametrized our new total $^{17}O(p,\alpha)^{14}N$ reaction rate in a widely utilized format,

$$N_A\langle\sigma v\rangle = \sum_{i=1}^{3} \exp\left[a_{i1} + \sum_{j=2}^{6} a_{ij} {T_9}^{2j/3-7/3} + a_{i7} \ln T_9\right], \tag{4}$$

from Ref. [19] using online tools available from the Computational Infrastructure for Nuclear Astrophysics (CINA) [20]. The coefficients in Eq. (4) determined from a best fit to our $^{17}O(p,\alpha)^{14}N$ reaction rate are given in Table II. We have also parametrized the $^{17}O(p,\gamma)^{18}F$ reaction rate from Ref. [9] using the same procedure, and the coefficients are given in Table III. These parametrizations are valid over the entire temperature range of 0.01–10 GK and deviate by less than 5% [2%] from the numerically integrated $^{17}O(p,\alpha)^{14}N$ [$^{17}O(p,\gamma)^{18}F$] rates at any temperature in this range.

We studied the impact of the new $^{17}O + p$ reaction rates on nucleosynthesis in nova models using the framework available through CINA. A "post-processing" approach similar to Ref. [21] was utilized following a reaction network through time profiles of temperature and density in 28 radial zones taken from one-dimensional hydrodynamic calculations of nova outbursts on 1.15, 1.25, and 1.35 solar mass ($M_{\odot}$) ONeMg white dwarf stars [22]. A full reaction network was used in each zone with 169 isotopes from ^{1}H to ^{54}Cr. Reaction rates were taken from the NACRE evaluation [17] where available and otherwise from the REACLIB database [19]. Models were also calculated by using the new $^{17}O(p,\alpha)^{14}N$ and $^{17}O(p,\gamma)^{18}F$ reaction rates as parametrized in Tables II and III with all other reaction rates unchanged. Final abundances in each case were determined by summing the contributions of each zone weighted by the total mass of the zone.

The ratios of the final ^{18}F abundances produced in models using the $^{17}O(p,\alpha)^{14}N$ and $^{17}O(p,\gamma)^{18}F$ reaction rates from Ref. [17] to the final abundances produced in models using the parametrized rates from this work are given in Table IV. We find models using the new rates to reduce the production of ^{18}F by a factor of 10 with hydrodynamic profiles from a 1.15 $M_{\odot}$ white dwarf. This is comparable to reductions in ^{18}F production by a factor of 7.9 reported from full hydrodynamical simulations on a 1.15 $M_{\odot}$ white dwarf [8]. However, the $^{17}O + p$ reaction rates have reduced influence on nucleosynthesis as the white dwarf mass increases. The new reaction rates reduce ^{18}F production by a factor of 2 in the 1.25 $M_{\odot}$ model and have a negligible effect on the 1.35 $M_{\odot}$ model. This results from the reaction sequence $^{16}O(p,\gamma)^{17}F(p,\gamma)^{18}Ne(\beta)^{18}F$ that bypasses ^{17}O and becomes more important for more energetic novae owing to the strong temperature dependence of the $^{17}F(p,\gamma)^{18}Ne$ reaction rate [13]. The much stronger influence of the $^{17}O + p$ reaction rates in lower mass progenitors results from the decreased $^{17}F(p,\gamma)^{18}Ne$ reaction rate relative to ^{17}F β decay in cooler models. Although this general trend seems robust, full hydrodynamical simulations over a range of progenitor trajectories are required to quantitatively understand the impact of the new reaction rates on potential γ-ray observations of novae.

TABLE III. The 21 coefficients a_{ij} used to parametrize the $^{17}O(p,\gamma)^{18}F$ rate via a fit of Eq. (4) to the tabulated rate from Ref. [9]. The parametrization is valid over the temperature range 0.01–10 GK and reproduces the tabulated rate to within 2% over this range.

$i \backslash j$	1	2	3	4	5	6	7
1	-9.18598×10^{2}	-2.28606×10^{0}	3.19374×10^{1}	1.31299×10^{3}	-6.56844×10^{2}	2.17931×10^{2}	-1.33934×10^{2}
2	-5.57168×10^{1}	-4.92403×10^{-1}	2.47608×10^{1}	7.43767×10^{1}	-4.97559×10^{1}	1.17175×10^{1}	1.83200×10^{1}
3	6.77712×10^{3}	-2.75532×10^{0}	8.93484×10^{2}	-1.05467×10^{4}	4.94580×10^{3}	-2.34713×10^{3}	1.84163×10^{3}

TABLE IV. Ratio of the final ^{18}F abundance produced in ONeMg nova models using the reaction rates from Ref. [17] to the final ^{18}F abundance in models using the rates from Tables II and III.

Mass	^{18}F ratio
1.15 $M_\odot$	10.2
1.25 $M_\odot$	2.0
1.35 $M_\odot$	1.0

It should be noted that the influence of the $^{17}O + p$ reaction rates is also sensitive to the somewhat uncertain rate of the $^{17}F(p,\gamma)^{18}Ne$ reaction.

Finally, we studied the effect of interferences between levels and of the $E_x = 5604.8$ MeV ($E_{c.m.} = -1.7$ keV) subthreshold state on uncertainties in the total $^{17}O(p,\alpha)^{14}N$ reaction rate using SAMMY. These effects have not previously been considered in a systematic manner. We find that any chosen combination of interferences between levels does not have a significant effect on the total $^{17}O(p,\alpha)^{14}N$ reaction rate for $T > 3 \times 10^7$ K (less than a 3% change in the total rate). The interference between 1^- states has more importance at lower temperatures, corresponding to $\pm 20\%$ ($\pm 5\%$) change in the total reaction rate at 1×10^7 K (2×10^7 K) with the adopted resonance energies and strengths. This uncertainty is significantly exacerbated if the uncertain properties of the $E_x = 5604.8$ MeV (1^-) subthreshold state are considered. In our parametrized rate, we have neglected this resonance as was done in previous evaluations; however, a reduced proton partial width of $\theta_p^2 < 0.01$ is not ruled out [23]. At this level, the subthreshold state can have a significant influence on the shape of the interference between 1^- levels and on the $^{17}O(p,\alpha)^{14}N$ reaction rate for $T < 3 \times 10^7$ K, making the rate uncertain by a factor of as much as 11 (2.3) at $T = 1 \times 10^7$ K (2×10^7 K). This uncertainty may be important for the operation of the CNO cycles in main sequence hydrogen burning.

V. CONCLUSION

We studied the $^1H(^{17}O,\alpha)^{14}N$ reaction and demonstrated a new technique that provides a sensitive approach for determining resonant properties in (p,α) reactions. We precisely measured the energy and strength of the 183 keV resonance in the $^{17}O(p,\alpha)^{14}N$ reaction and find good agreement with a recently reported study [8,9]. We also report the first measurements of stopping powers for oxygen ions in hydrogen gas near the peak of the Bragg curve. We calculated the total $^{17}O(p,\alpha)^{14}N$ reaction rate using an R-matrix formalism and the new properties for the 183 keV resonance, and we parametrized the new rate in a commonly used format. Our reaction rate is in good agreement with Ref. [9] but substantially larger than the rate recommended by Ref. [17] at nova temperatures. Significant uncertainties remain in the $^{17}O(p,\alpha)^{14}N$ reaction rate only at the lowest temperatures ($T < 3 \times 10^7$ K) owing to the interference between 1^- resonances and the contributions of subthreshold states. Reaction network calculations were presented that show the new $^{17}O(p,\alpha)^{14}N$ reaction rate to decrease ^{18}F production significantly in some ONeMg novae, though there is less influence on the most energetic novae where the $^{17}F(p,\gamma)^{18}Ne$ reaction bypasses ^{17}O production. We now propose to apply this new experimental technique to measure the strength of low-energy resonances in the $^{18}F(p,\alpha)^{15}O$ reaction, which is also important for understanding novae and γ-ray production from the decay of ^{18}F.

ACKNOWLEDGMENTS

The authors thank Sumner Starrfield for supplying the hydrodynamic profiles for ONeMg novae. The authors also thank the staff of the HRIBF whose efforts produced high-quality ^{17}O beams despite operating the HRIBF tandem at record low voltages of about 1.5 MV. ORNL is managed by UT-Battelle, LLC, for the U.S. Department of Energy under Contract No. DE-AC05-00OR22725. This work was supported in part by the U.S. Department of Energy under Grant Nos. DE-FG03-93ER40773, DE-FG02-96ER40955, DE-FG02-93ER40789, DE-FG02-96ER40990, and DE-FG02-88ER40387.

[1] M. J. Harris and D. L. Lambert, Astrophys. J. **285**, 674 (1994).
[2] L. R. Nittler, C. M. O'D. Alexander, X. Gao, R. M. Walker, and E. Zinner, Astrophys. J. **483**, 475 (1997).
[3] D. S. P. Dearborn, Phys. Rep. **210**, 367 (1992).
[4] A. I. Boothroyd and I.-J. Sackmann, Astrophys. J. **510**, 232 (1999).
[5] L. R. Nittler and R. Cowsik, Phys. Rev. Lett. **78**, 175 (1997).
[6] J. José and M. Hernanz, Astrophys. J. **494**, 680 (1998).
[7] M. Hernanz and J. José, New Astron. Rev. **48**, 35 (2004).
[8] A. Chafa *et al.*, Phys. Rev. Lett. **95**, 031101 (2005); **96**, 019902(E) (2006).
[9] A. Chafa *et al.*, Phys. Rev. C **75**, 035810 (2007).
[10] C. Fox *et al.*, Phys. Rev. Lett. **93**, 081102 (2004).
[11] C. Rolfs, I. Berka, and R. E. Azuma, Nucl. Phys. **A199**, 306 (1973).
[12] C. Fox *et al.*, Phys. Rev. C **71**, 055801 (2005).
[13] D. W. Bardayan *et al.*, Phys. Rev. C **62**, 055804 (2000).
[14] J. F. Ziegler, computer code SRIM-2003.10 (2003); see http://www.srim.org.
[15] H. Paul and A. Schinner, At. Data Nucl. Data Tables **85**, 377 (2003). Available from http://www-nds.iaea.org/stoppinggraphs.
[16] N. M. Larson, Oak Ridge National Laboratory Report No. ORNL/TM-9179/R7, 2006.
[17] C. Angulo *et al.*, Nucl. Phys. **A656**, 3 (1999).
[18] C. Rolfs, W. E. Kieser, R. E. Azuma, and A. E. Litherland, Nucl. Phys. **A199**, 274 (1973).
[19] T. Rauscher and F.-K. Thielemann, At. Data Nucl. Data Tables **79**, 47 (2001).
[20] M. S. Smith *et al.*, in proceedings of the "International Symposium on Nuclear Astrophysics—Nuclei in the Cosmos—IX," PoS (NIC-IX) 180; http://www.nucastrodata.org.
[21] S. Parete-Koon *et al.*, Astrophys. J. **598**, 1239 (2003).
[22] S. Starrfield *et al.*, Mon. Not. R. Astron. Soc. **296**, 502 (1998).
[23] V. Landre *et al.*, Phys. Rev. C **40**, 1972 (1989).